Surface lattice dynamics of KCl(001): A high-resolution helium atom scattering study

Rifat Fatema, David H. Van Winkle,* and J. G. Skofronick
MARTECH and Department of Physics, Florida State University, Tallahassee, Florida 32306-4350, USA

Sanford A. Safron
MARTECH and Department of Chemistry and Biochemistry, Florida State University, Tallahassee, Florida 32306-4390, USA

F. A. Flaherty
Department of Physics, Valdosta State University, Valdosta, Georgia 31698-0055, USA
(Received 1 August 2007; published 14 January 2008)

High-resolution helium atom scattering has been employed to investigate the surface lattice dynamics of the KCl(001) surface. Several branches of surface phonon dispersion have been mapped across the surface Brillouin zone in the $\overline{\Gamma M}$ and $\overline{\Gamma X}$ high symmetry directions. These branches include the low-energy Rayleigh wave, crossing branches which increase in energy from the surface Brillouin zone boundary to the zone center, and a dispersionless optical branch. The results are compared with previously reported calculations based on the shell model and with earlier experimental results for surface and bulk phonon dispersions in KCl.

DOI: 10.1103/PhysRevB.77.024305 PACS number(s): 61.05.Np, 63.20.−e, 68.49.Bc

I. INTRODUCTION

We report data on the lattice dynamics of the KCl(001) surface at sufficient resolution to show that, for the most part, the measured low-energy surface phonons agree well with both bulk shell model calculations and surface model behavior. The lattice dynamics of the alkali hallide (001) surfaces have been investigated in great detail both theoretically and experimentally. In 1978, Benedek and co-workers used a Green's function approach to calculate the surface localized phonons and resonances for many of these systems.[1,2] In this same period, de Wette and co-workers presented a comprehensive study of the surface lattice dynamics of the materials by employing a "slab dynamics" calculation.[3,4] Helium atom scattering (HAS) experiments pioneered by the Göttingen group[5,6] in Germany, and also carried out by the FSU group in Tallahassee, Florida, measured the surface phonon dispersion for ten of these crystalline materials, which could be compared directly with these calculations.[7] Despite very good agreement, in general, features not apparent in the theoretical work were found in a few of these experiments.[8,9]

Foldy and co-workers have pointed out the "extended symmetry" that occurs in the bulk phonon dynamics of isobaric alkali halide crystals such as KCl.[10,11] These authors noted the near degeneracy of certain bulk phonon dispersion branches at the Brillouin zone boundaries, which results from the similarity of the ionic masses and the absence of distinct molecular units in these materials. Benedek and coworkers have pointed out that aspects of this effect should also be evident in the surface phonon dispersion branches for KCl.[2,9,12] In particular, one would predict a surface branch with optical mode characteristics, which appears as a "folded" extension of the Rayleigh wave at the boundaries of $\overline{\Gamma M}$ and $\overline{\Gamma X}$ regions of the surface Brillouin zone (SBZ). A similar-appearing optical branch, called a "crossing mode," was seen in measurements and in some calculations for the nonisobaric KBr(001) surface.[8,9] For KCl(001), both theoretical treatments predict the existence of such a branch.

Previous HAS measurements have been carried out on KCl(001) only for the $\overline{\Gamma M}$ region of the SBZ.[5,6] The results reported for the Rayleigh wave are in good agreement with the calculations and a few data points were obtained that matched the folded or crossing branch. More recently, HAS has been used for studying other types of surfaces. For example, HAS experiments have been performed using KCl as a substrate for a deposited acetylene surface.[13,14] Similarly, we used KCl as a substrate for deposited amino acids. As a precursor, we measured the dynamics of the KCl(001) surface in both $\overline{\Gamma M}$ and $\overline{\Gamma X}$ regions of the SBZ. We have obtained extensive data for the Rayleigh wave and crossing branch in each region. In $\overline{\Gamma M}$, we have also obtained several points in the energy range of the higher lying Lucas mode (S_4 and S_5 branches). However, the values we have found lie very close to the calculated S_5 (shear horizontal) branch rather than to the S_4 (sagittal plane) branch. The polarization of the S_5 branch phonons is prevented by symmetry from coupling to the helium scattering. Thus, there appears to be some disagreement between the model calculations and the experiments for higher-energy vibrational modes.

II. HELIUM ATOM SCATTERING APPARATUS

The FSU HAS instrument has been described in considerable detail in previous publications.[7,8,15] Briefly, the instrument consists of three main sections: (i) a beam source chamber, (ii) a scattering chamber, and (iii) time-of-flight (TOF) and detector chambers. A nearly monoenergetic ($\Delta E/E \approx 2\%$) helium atom beam is produced by expanding the helium gas at ~25–30 bar pressure from a nominal 30 μm nozzle and then passing it through a 1 mm skimmer. The temperature of the nozzle can be varied from about 80 to 325 K, resulting in atom energies ranging from 18 to 67 meV. For TOF measurement of the inelastic helium atom-surface scattering, a beam chopper, consisting of a 145 mm diameter wheel with eight equally spaced, 1 mm wide slits, is inserted into the beam path. The chopper pro-

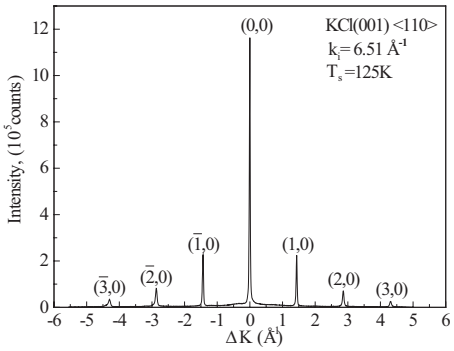

FIG. 1. Typical angular distribution (AD) for KCl(001) in the ⟨110⟩ direction; surface temperature T_s=125 K and incident wave vector k_i=6.51 Å^{-1}. The central peak at ΔK=0 is the specular reflection with symmetric Bragg peaks flanking either side. The labels on the peaks are the (n,m) values of the surface reciprocal lattice vector $\mathbf{G}_{n,m}$.

vides pulses of helium atoms with full width at half maximum of ~30 μs. For elastic helium atom-surface scattering experiments, the chopper is withdrawn from the beam path to illuminate the target with the full, continuous helium beam.

The beam passes through a differentially pumped region before entering the scattering chamber and striking the target at an incident angle θ_i. The target sample is mounted onto a manipulator equipped for alignment with an x,y,z translational stage, two rotational adjustments, and a tilting stage. The helium atoms scatter from the target in all directions. Those reflected in the plane defined by the nozzle-target axis and the target-detector axis are able to travel through the TOF section to the detector. From the fixed 90° geometry of the instrument, the scattering angle θ_f=90°−θ_i. At the entrance to the detector, the atoms pass through an ionizer (electron bombardment) region; then, they are transmitted through a quadrupole mass spectrometer and, finally, are counted by standard electron-pulse counting techniques. Helium atoms not ionized by the electron bombarder passed straight through the chamber and are pumped away in a "sump" section.

III. EXPERIMENTAL MEASUREMENTS

A. Elastic scattering

Helium atom diffraction from the target surface is obtained by an angular distribution (AD) measurement. This is carried out by measuring the total scattered atom intensity at each angle θ_f as the target mounted on the manipulator is rotated by a stepping motor. A typical AD is shown in Fig. 1 for KCl(001) in the ⟨110⟩ azimuth. Peaks in the AD are found at angles where the Bragg diffraction condition, $\Delta\mathbf{K}=\mathbf{G}_{n,m}$, is satisfied. Here, $\Delta\mathbf{K}=\mathbf{K}_f-\mathbf{K}_i=k_f\sin\theta_f-k_i\sin\theta_i$ is the difference between the final and initial helium atom wave vector components (k_f,k_i) parallel to the surface $(\mathbf{K}_f,\mathbf{K}_i)$, and $\mathbf{G}_{n,m}$ is a surface reciprocal lattice vector. For elastic scattering and our 90° geometry, the magnitude of $\Delta\mathbf{K}$ becomes $\Delta K=\sqrt{2}k_i\cos(\theta_i+45°)$.

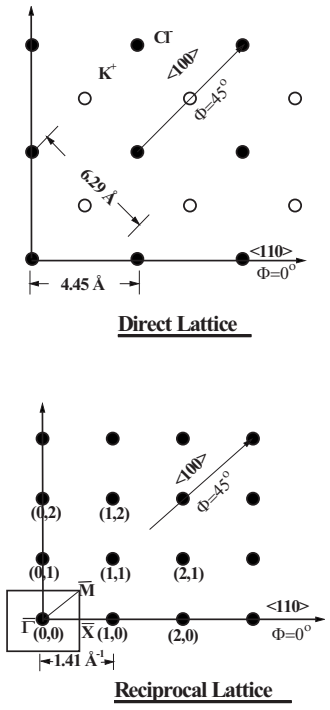

FIG. 2. Representation of the direct lattice (upper panel) and reciprocal lattice (lower panel) of KCl(001), illustrating the relative orientations of the high symmetry directions: ⟨110⟩ and ⟨100⟩. The first surface Brillouin zone (SBZ) is the square box around the point $\bar{\Gamma}$ in the lower panel and the triangular region $\overline{\Gamma MX}$ constitutes an irreducible region of the SBZ.

Figure 2 shows the direct and reciprocal lattices for the KCl(001) crystal. The Bragg peaks shown in Fig. 1 correspond to the reciprocal lattice points in the lower panel of Fig. 2. The irreducible SBZ, defined as the smallest portion of the first Brillouin zone containing all of the symmetries in the point group of the lattice, is also shown in Fig. 2 as the triangular region $\overline{\Gamma MX}$.

B. Inelastic scattering

Under the operating conditions of our instrument, the inelastically scattered helium atoms are scattered principally by single phonon creation or annihilation events at the surface.[5] An example of a TOF spectrum is given in Fig. 3. From the elastic arrival times and the incident angle, one can convert the TOF spectrum to an energy transfer spectrum (also shown in Fig. 3). The peaks in each spectrum ultimately become points in a plot of energy transfer $(\Delta E=E_f-E_i)$ against parallel momentum transfer (ΔK), as shown in Fig. 4. That is, the peaks in the TOF spectra correspond to surface phonons with energies $\hbar\omega=\Delta E$ and wave vectors $\mathbf{Q}$ obtained from $\Delta\mathbf{K}=\mathbf{G}_{n,m}+\mathbf{Q}$.

Each TOF experiment is carried out at a fixed initial energy E_i, wave vector k_i $(E_i=\hbar^2k_i^2/2m)$, and incident angle θ_i. Only surface phonons which lie on the "scan curve" determined by the combination of energy and momentum conservation constraints,[5]

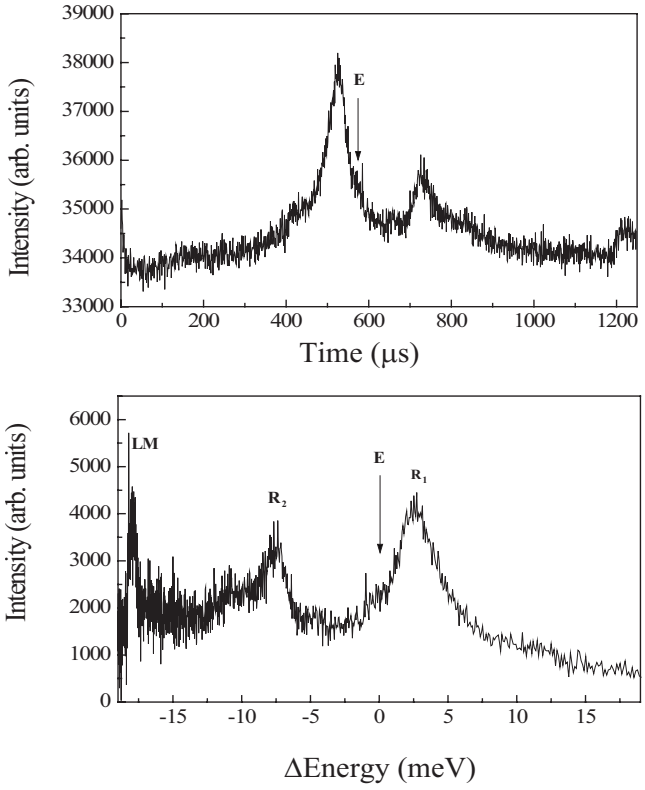

FIG. 3. The upper panel shows the TOF spectrum taken at $\theta_i = 37°$ from KCl(001) in the ⟨100⟩ high symmetry direction with surface temperature $T_s = 150$ K and $k_i = 7.25$ Å^{-1}. In the lower panel, the TOF spectrum has been converted to an energy transfer distribution; the peak intensities are modified by the Jacobian of the arrival time to energy transfer conversion. R_1 and R_2 label peaks correspond to Rayleigh mode phonons, LM labels the Lucas mode phonon peak, and E at $\Delta E = 0$ marks the peak due to diffuse elastic scattering.

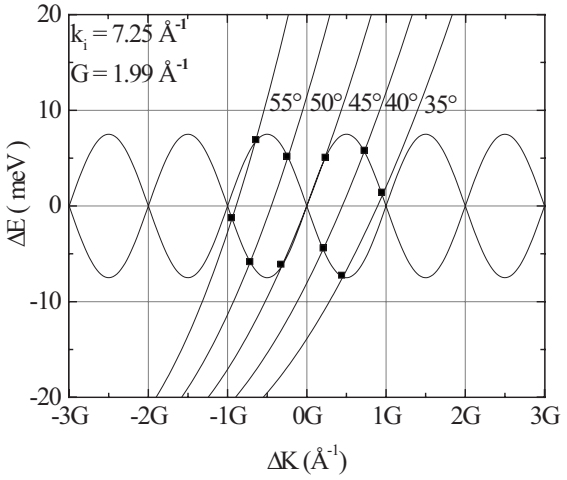

FIG. 4. Scan curves for incident angles of 35° to 55° for a beam with incident wave vector $k_i = 7.25$ Å^{-1}. The sine wave represents the model Rayleigh wave dispersion branch in an extended SBZ plot. The intersections (solid squares) show the $(\Delta E, \Delta K)$ phonons that could be observed in a TOF spectrum measured at each θ_i.

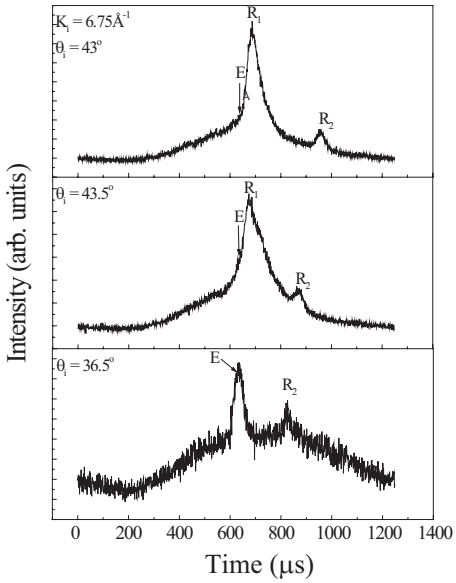

FIG. 5. Selected TOF spectra from KCl(001) in the ⟨110⟩ high symmetry direction with surface temperature $T_s = 200$ K and incident wave vector $k_i = 6.75$ Å^{-1}. R_1 and R_2 correspond to Rayleigh phonon modes and E marks the elastic arrival time.

$$\frac{\hbar\omega}{E_i} = \left[\frac{K_i + \Delta K}{k_i \cos\theta_i}\right]^2 - 1 \tag{1}$$

can be observed.

The peaks in a TOF spectrum for each θ_i correspond to intersections of the scan curve with the surface phonon dispersion curves. This is schematically shown in Fig. 4 in an extended SBZ plot of ΔE vs ΔK: the scan curves for five different incident angles intersect with sinusoidal curves representing phonon dispersion curves. Hence, TOF spectra measured over a range of incident angles provide a way to determine the surface phonon dispersion branches.

IV. RESULTS

A total of 87 TOF spectra were obtained in the ⟨110⟩ and ⟨100⟩ high symmetry azimuths for the KCl(001) surface. In the ⟨110⟩ azimuth, spectra were obtained for incident angles from 30° to 52°, and in the ⟨100⟩ azimuth for incident angles from 32.5° to 53.5°. In these experiments, the incident wave vectors ranged from 6.57 to 7.32 Å^{-1}. Examples of spectra in each azimuth are presented in Figs. 5 and 6.

From the peaks in all the spectra, the surface phonon energies and wave vectors have been evaluated and are plotted in Figs. 7 and 8 for comparison with the calculated surface phonon dispersion for KCl by Kress *et al.* (Fig. 7) and by Benedek and co-workers (Fig. 8). For alkali halides with the rocksalt structure, such as KCl, the data in the ⟨100⟩ azimuth correspond to surface dispersion points for the region $\overline{\Gamma M}$ of the SBZ and the data in the ⟨110⟩ azimuth for the region $\overline{\Gamma X}$ of the SBZ (as shown in Fig. 2).

We note that peaks were found in several spectra (e.g., in Fig. 6) which corresponded to "deceptons" rather than phonons. These false peaks have been seen in HAS experi-

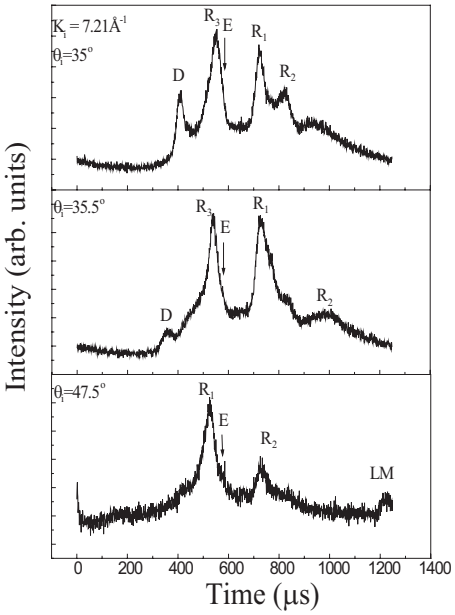

FIG. 6. Selected TOF spectra from KCl(001) in the ⟨100⟩ high symmetry direction with surface temperature $T_s = 125$ K and incident wave vector $k_i = 7.21$ Å^{-1}. R_1, R_2, and R_3 correspond to Rayleigh phonon modes, E marks the elastic arrival time, LM is a Lucas mode phonon, and D is a decepton as described in the text.

ments on LiF(001) and NaF(001) (Ref. 5) and arise from the elastic, diffractive scattering of helium atoms with wave vectors in the "tails" of the beam speed distribution. They can occur in TOF spectra taken at incident angles close to the positions of the Bragg diffraction peaks.

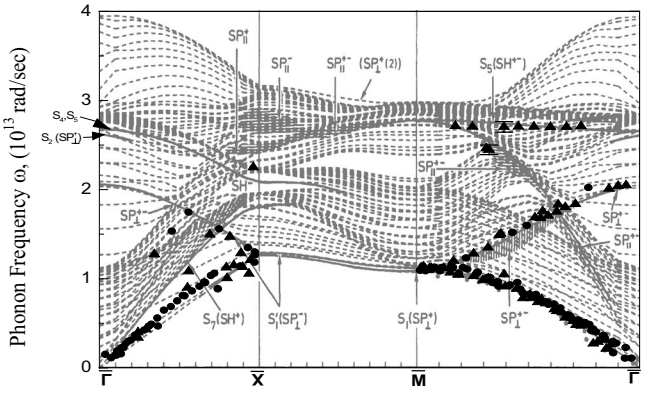

FIG. 7. Comparison of measurements with the surface phonon dispersion curves for KCl(001) calculated by Kress *et al.* (Ref. 4). The black circles and triangles correspond to good and average quality experimental points, respectively, from this work; the dispersion curves calculated by the slab dynamics approach are shown in gray; the previously measured points by Kress *et al.* and Doak and co-workers (Refs. 4–6) in $\overline{\Gamma M}$ are also shown as gray dots. Error bars are included for two high-energy points in $\overline{\Gamma M}$ to indicate the uncertainty in these measurements; error bars for the Rayleigh and crossing mode points are comparable to the size of the symbols shown.

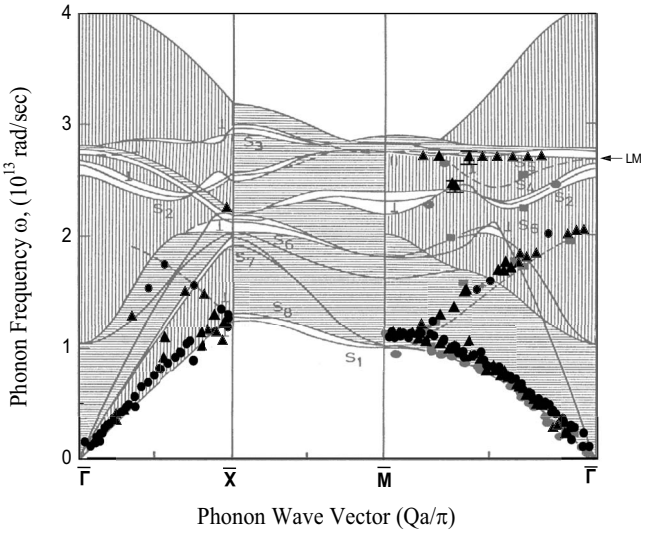

FIG. 8. Comparison of measurements with the surface phonon dispersion curves for KCl(001) calculated by Benedek and coworkers (Ref. 19). Their Green's function calculations are shown in gray. The data points shown are as in Fig. 7.

V. DISCUSSION

A. Comparison with calculations

For comparison of the measured dispersion data with the theoretical calculations, we have plotted our points in Fig. 7 onto the slab dynamics calculation of the surface phonon dispersion curves of Kress *et al.*[4] and in Fig. 8 onto the Green's function calculation by Benedek and co-workers.[18,19] Both theoretical approaches employ the shell model to represent the interactions of the K^+ and Cl^- ions in determining the surface phonon dispersion. The work of Kress *et al.* also allowed for surface relaxation.

In general, agreement between the model calculations and the measurements is rather good for the Rayleigh wave and for the crossing mode. In Fig. 7, one can see that the agreement for both these branches in $\overline{\Gamma M}$ is very close, but for the Rayleigh wave in $\overline{\Gamma X}$, the measured values are a bit higher than the calculations. In Fig. 8, the measured Rayleigh wave points lie slightly higher in energy than the calculated curves in both $\overline{\Gamma M}$ and $\overline{\Gamma X}$, as the crossing branch points in $\overline{\Gamma M}$ do. These small differences, however, do not detract from the generally satisfying match between the model calculations and the experiment.

For the higher-energy surface phonons in $\overline{\Gamma M}$ near the Lucas mode, the situation is less clear. The S_4 and S_5 surface phonon branches are degenerate at the $\bar{\Gamma}$ point, but diverge across the $\overline{\Gamma M}$ region of the SBZ. In Figs. 7 and 8, one can see that the measured points appear to follow the nearly dispersionless S_5 branch rather than S_4. This is surprising. The S_4 branch is polarized in the sagittal plane and, therefore, can be observed, in principle, by helium atom scattering. In contrast, the S_5 branch is polarized shear horizontally and by symmetry cannot couple to the scattered helium atoms in our experimental geometry. We note that whereas S_4 is marked in Fig. 8 as a surface resonance that drops below S_5 in the

central portion of $\overline{\Gamma M}$, in Fig. 7, Kress *et al.* have not actually indicated where the calculated S_4 branch occurs. This difference may reflect some indeterminacy in the model calculations for this branch.

B. Extended symmetry

Extended symmetry for isobaric rocksalt-structured alkali halides such as KCl can be understood more easily by examining the bulk and surface Brillouin zones shown in Fig. 9. If the masses of K^+ and Cl^- were exactly the same and the ionic interactions completely interchangeable between the positive and negative ions, bulk KCl would effectively appear as a monatomic crystal with a simple cubic unit cell, having a lattice constant half that of the true fcc KCl crystal. Its Brillouin zone (BZ) would then be a cube that encloses the true fcc BZ, as shown in Fig. 9(a). One can see from the figure that the corners of the cube lie at the zone centers of the neighboring fcc BZs.

For a simple cubic crystal, only three acoustic phonon branches should exist. However, from the extended symmetry, the wave vectors in the cube lying outside the true BZ may be mapped into the true zone, so that the corresponding acoustic phonons of the extended zone become the bulk optical modes of the true BZ. In particular, the hexagonal faces of the fcc BZ can be seen to be folding planes for these phonon branches. In the high symmetry direction (ζ,ζ,ζ), where ζ is the reduced coordinate [i.e., along ΓL in Fig. 9(a)], the point L is halfway from Γ in the first true BZ to the Γ of the next BZ at the corner of the cube. The optical modes of the isobaric crystal in ΓL, then, correspond to the extended acoustic modes folded into the true zone about L. Foldy and co-workers have noted the near degeneracy of the longitudinal acoustic (LA) and optical (LO) modes and of the transverse acoustical (TA) and optical (TO) modes at L for the nearly isobaric alkali halides NaF, KCl, and RbBr.[10,11] This can be seen in the phonon dispersion curves for KCl from neutron scattering experiments shown in Fig. 9(c).[16,17]

The optical modes in the other fcc BZ high symmetry directions $(\zeta,\zeta,0)$ and $(\zeta,0,0)$ can be seen to correspond to wave vectors at the boundaries of the extended simple cubic BZ. Along the direction $(\zeta,\zeta,0)$, these wave vectors lie on a line connecting a corner of the cube (a Γ point of a neighboring fcc BZ) to the center of one of its adjacent faces (an X point). Along the direction $(\zeta,0,0)$, these wave vectors lie along an edge of the cube from one corner (a Γ point) to halfway to the next corner (an X point in a neighboring fcc BZ).

For the (001) surface of a rocksalt-structured crystal, the irreducible portion $(\overline{\Gamma XM})$ of the extended two-dimensional SBZ can be represented as in Fig. 9(b), where to provide orientation, the corresponding fcc bulk BZ point labels [as in Fig. 9(a)] are shown in parentheses next to the true SBZ points. Note that the SBZ points $\bar{\Gamma}$ and $\bar{M}$ correspond to Γ and X, respectively, in the true bulk BZ [i.e., in the $(\zeta,0,0)$ high symmetry direction]. The SBZ point $\bar{X}$ lies in the $(\zeta,\zeta,0)$ high symmetry direction below L, and the $\bar{\Gamma}$ point in the second SBZ corresponds to the point X in the next fcc BZ. With respect to the extended simple cubic BZ, $\bar{M}$ (at X) lies in the center of a face of the cube and $\bar{\Gamma}$ of the next SBZ lies at the midpoint of an edge (also an X point).

By analogy to folding planes in the three-dimensional case, symmetry requires the line $\overline{XM}$ to be a folding line. Hence, one might expect crossing modes to arise in $\overline{\Gamma X}$ from bulk acoustic phonon branches in ΓX folded about $\bar{X}$. One can identify the vibrational frequency of the folded transverse branch at the surface zone center $(\bar{\Gamma})$ as that of the LA mode at the bulk X point for KCl, $\sim 2.04\times 10^{13}$ rad/s. Similarly, one can identify the crossing branch in $\overline{\Gamma M}$ with the modes in the cubic face of the fcc BZ along the line that runs from X $(\bar{M})$ to W to X $(\bar{\Gamma})$, and the frequency of this phonon branch at $\bar{\Gamma}$ should again be that of the LA mode at X.

Because of the broken symmetry in the forces at a surface, these surface vibrations can merge with bulk modes of the same polarization and lose their distinction as surface localized modes or resonances. Benedek and co-workers have shown that crossing modes are observed only in the alkali halides, such as KCl, for which the hybridization of the LA and LO modes leads to a structure-induced surface resonance.[9,12] In these cases, the density of states at the surface becomes large enough for the mode to exist as a distinct surface resonance.

For KCl, the surface vibrational modes observed in the experiments reported here are found to agree very well, as predicted, with the bulk mode frequencies. In Fig. 10, we have plotted our data onto the reported bulk dispersion curves for KCl from neutron scattering experiments in Fig. 9(c) after folding the bulk curves into the SBZ, as indicated above. The very good agreement seen for the low-energy modes breaks down only slightly for the bulk optical modes. This suggests that the forces acting on the surface K^+ and Cl^- ions cannot be very different from those of the ions in the bulk of this material. This somewhat surprising result is, however, consistent with the calculations of Kress *et al.*,[4] which show significant surface relaxation only for the more massive and polarizable alkali halides, RbBr and RbI.

VI. CONCLUSION

The measurements of the surface lattice dynamics of KCl(001) have been found to be in reasonably good agreement with the shell model calculations for the Rayleigh wave in both $\overline{\Gamma M}$ and $\overline{\Gamma X}$ regions of the SBZ. The agreement is also relatively good for the crossing branch. However, HAS appears insensitive to the optical mode vibrations of KCl(001) except, apparently, to the Lucas mode in $\overline{\Gamma M}$. For the Lucas mode, however, there seems to be disagreement between both sets of calculations[4,18,19] and our experimental results. Further, calculations shown in Fig. 8 indicate the existence of a perpendicularly polarized optical branch S_2 lying in a narrow band gap that should be observable by helium scattering experiments. This branch was not observed in our scattering experiments. However, since the surrounding bulk-projected bands are similarly polarized, inelastic helium scattering from these vibrational modes may "smear

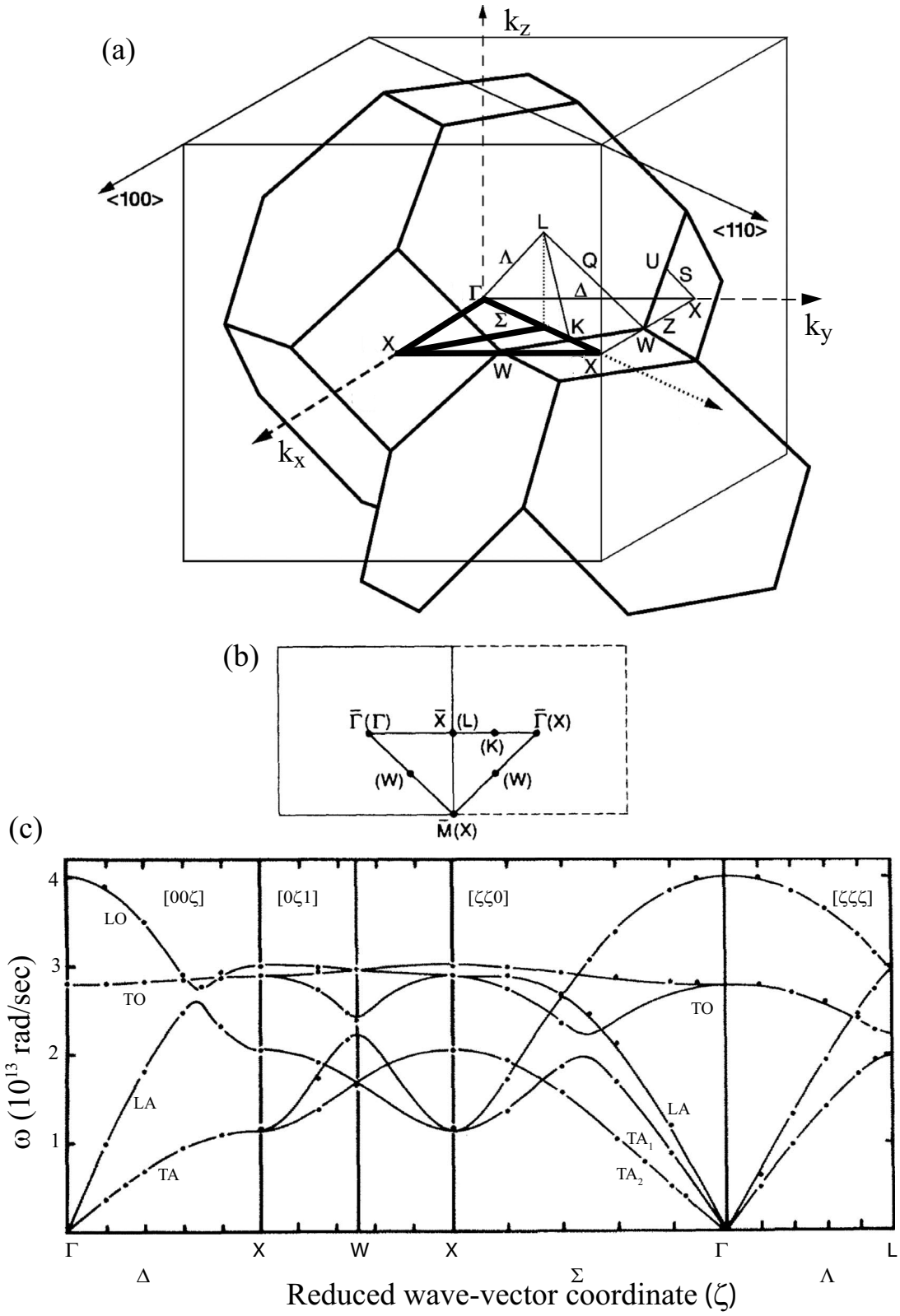

FIG. 9. (a) Brillouin zone (BZ) for fcc crystals, illustrating the relation between the true fcc BZ and the extended symmetry simple cubic BZ. The high symmetry points and regions of the true BZ are indicated, and a portion of a neighboring fcc BZ is included. The region bound by heavy lines corresponds to the irreducible portions of the surface Brillouin zone shown in (b) (adapted from Ref. 9). (b) SBZ for KCl(001) is shown as the solid line square and a neighboring SBZ as the dashed line square. The high symmetry points are indicated, with the corresponding three-dimensional points from (a) shown in parentheses (adapted from Ref. 9). (c) Phonon dispersion curves for KCl (adapted from Ref. 16).

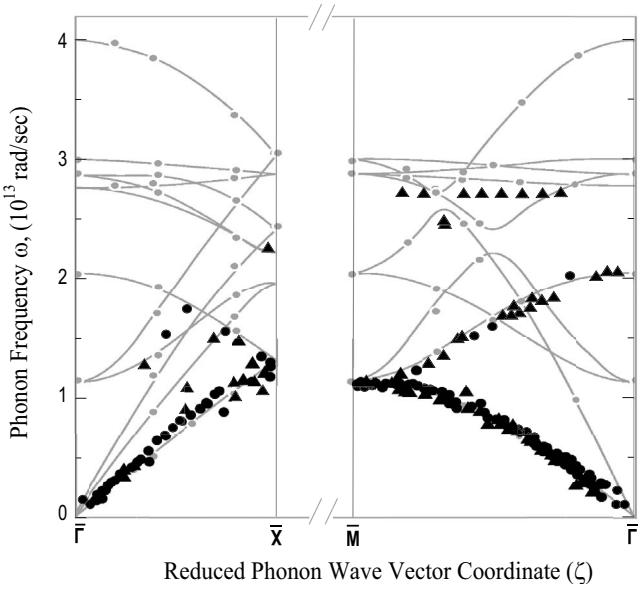

FIG. 10. Comparison of the surface phonon measurements of KCl(001), as in Figs. 8 and 9, with the folded phonon dispersion curves for bulk KCl from Ref. 16 [as shown in Fig. 9(c)], as described in the text. The black circles and triangles correspond to good and average quality experimental points, respectively, from this work.

out" the TOF intensities enough to prevent the scattering from the S_2 modes appearing as identifiable TOF peaks. On the other hand, the calculations in Fig. 7 do not show this S_2 surface branch in $\overline{\Gamma M}$. This disagreement between the calculational approaches suggests that some additional theoretical work may be needed to resolve these discrepancies.

The measured Rayleigh and crossing mode dispersion closely matches that of the folded fcc TA branches. This suggests that the forces on the ions at the KCl(001) surface associated with these sagittal plane vibrations cannot be very different from the forces on the ions in the bulk associated with the corresponding transverse acoustic vibrations. The calculations of Kress *et al.* indicate little surface relaxation for KCl(001). This also indicates that the net forces on the ions are similar in the bulk and at the surface. This agreement between the dispersion of the measured surface phonons and the bulk phonons also suggests that extended symmetry can be useful in making sense of the underlying physics of similar phenomena.

ACKNOWLEDGMENTS

We gratefully acknowledge the support of this research by MARTECH and Florida State University.

*rip@phy.fsu.edu

[1] G. Benedek and F. Galimberti, Surf. Sci. **71**, 87 (1978); **118**, 713(E) (1982).
[2] G. Benedek and L. Miglio, in *Ab-Initio Calculation of Phonon Spectra*, edited by J. Devreese (Plenum, New York, 1982).
[3] T. S. Chen, F. W. de Wette, and G. P. Alldredge, Phys. Rev. B **15**, 1167 (1977).
[4] W. Kress, F. W. de Wette, A. D. Kulkarni, and U. Schröder, Phys. Rev. B **35**, 5783 (1987).
[5] G. Brusdeylins, R. B. Doak, and J. P. Toennies, Phys. Rev. B **27**, 3662 (1983).
[6] R. B. Doak, Ph.D. thesis, Massachusetts Institute of Technology, 1981.
[7] For a review, see S. A. Safron, *Advances in Chemical Physics*, edited by I. Prigogine and Stuart A. Rice (Wiley, New York, 1996), Vol. XCV, p. 129.
[8] G. Chern, J. G. Skofronick, W. P. Brug, and S. A. Safron, Phys. Rev. B **39**, 12828 (1989).
[9] S. A. Safron, G. Chern, W. P. Brug, J. G. Skofronick, and G. Benedek, Phys. Rev. B **41**, 10146 (1990).
[10] L. L. Foldy and T. A. Witten, Jr., Solid State Commun. **37**, 709 (1981).
[11] B. Segall and L. L. Foldy, Solid State Commun. **47**, 593 (1983).
[12] G. Benedek, L. Miglio, G. Brusdeylins, J. G. Skofronick, and J. P. Toennies, Phys. Rev. B **35**, 6593 (1987).
[13] J. P. Toennies, F. Traeger, H. Weiss, S. Picaud, and P. N. M. Hoang, Phys. Rev. B **65**, 165427 (2002).
[14] A. L. Glebov, V. Panella, J. P. Toennies, F. Traeger, H. Weiss, S. Picaud, P. N. M. Hoang, and C. Girardet, Phys. Rev. B **61**, 14028 (2000).
[15] E. A. Akhadov, S. A. Safron, J. G. Skofronick, D. H. Van Winkle, F. A. Flaherty, and Rifat Fatema, Phys. Rev. B **68**, 035409 (2003).
[16] G. Raunio and S. Rolandson, Phys. Rev. B **2**, 2098 (1970).
[17] G. Raunio and L. Almqvist, Phys. Status Solidi **33**, 209 (1969).
[18] G. Benedek, G. Brusdeylins, R. B. Doak, and J. P. Toennies, J. Phys. (Paris), Colloq. **42**, C6 (1981).
[19] L. Miglio and G. Benedek, in *Structure and Dynamics of Surfaces II*, edited by W. Schommers and P. von Blanckenhagen (Springer, Heidelberg, 1987), p. 35.